Trapped Image Guide for Millimeter-Wave Circuits

TATSUO ITOH, SENIOR MEMBER, IEEE, AND BERND ADELSECK

Abstract—**A novel dielectric waveguide is proposed for use in millimeter-wave integrated circuits, and a simple analysis for dispersion characteristics is developed. Numerical results agree reasonably with measured data. Radiation losses of this waveguide at curved sections are proven to be considerably less than those of the image guide. As an application of this waveguide, a leaky-wave radiator has been tested.**

I. Introduction

RECENTLY, a number of works have been reported on millimeter-wave integrated circuits based on dielectric waveguides [1], [2]. In addition to image guide structures, several new waveguides have been proposed and tested [1], [3], [4]. An inherent problem of dielectric waveguides is the loss due to radiation at curved sections, junctions and discontinuities. This problem may be alleviated by the use of materials with high permittivities. However, use of such materials is often prohibited due to operating frequencies, sizes, and so on.

This paper proposes a new type of open dielectric waveguide which reduces the radiation loss at curved sections in dielectric integrated circuits. The structure is called a trapped image guide and is essentially a rectangular dielecric rod placed in a metal trough. The cross section of the trapped image guide is depicted in Fig. 1. In integrated circuit applications, almost all the bends are in the sideward direction. In ordinary image guides, the electromagnetic energy escapes from the guide as a propagating wave in the sideward direction at the bend. In the trapped image guide, such a leakage will be mostly reflected back to the dielectric portion by the metal walls if their height (the depth of the trough) h is reasonably large. As long as the waveguide is operated in the single mode region, the reflected energy will couple to the guided mode once again. Of course, an excessively large h is not very practical in actual integrated circuit applications. The trough may be readily created by machining a metal plate. An alternative is to machine a trough in a dielectric material followed by a metal plating.

Actual *Ka*-band (26.5–40 GHz) test setups of straight and curved sections of trapped image guide are photographed in Fig. 2. In these setups, instead of a machined trough, we added metal side walls to the ground plane for an image guide. Metal side walls to create the trough may be removed when an image guide setup is desired. Two transitions are provided for connecting the setups to conventional rectangular metal waveguides. Each of these transitions includes a semiconical horn originally designed for image guides (Fig. 2 without side walls) and tapers on the metal side walls to provide smooth transition to the trapped image guide. In what follows, we provide an approximate theoretical analysis of waveguiding char-

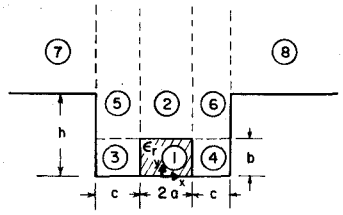

Fig. 1. Cross section of the trapped image guide.

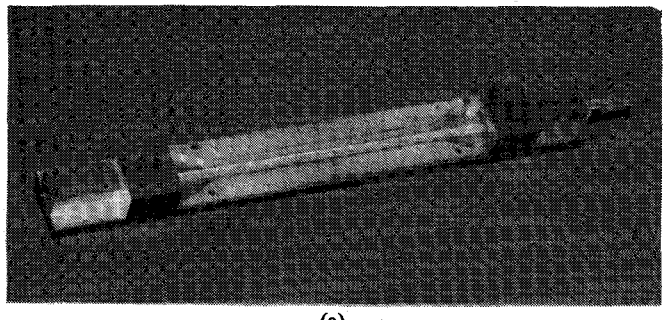

(a)

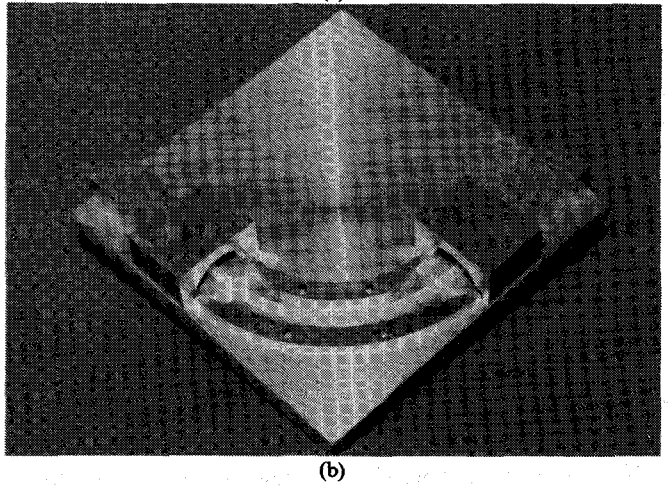

(b)

Fig. 2. Trapped image guide structures.

Manuscript received May 16, 1980. This work was supported by the U.S. Army under Research Grant DAAG29-78-G-0145.

T. Itoh is with the Department of Electrical Engineering, The University of Texas at Austin, Austin, TX 78712.

B. Adelseck is with AEG-Telefunken, Hoch-frequenztechnik D-7900, Ulm, West Germany.

0018-9480/80/1200-1433$00.75 ©1980 IEEE

acteristics in the trapped image and the results are compared with experimental data. Some experimental investigations on the radiation loss characteristics at the bend are reported. An application of this waveguide as a frequency-scannable leaky-wave radiator is included.

II. Analysis of the Propagation Characteristics

The complete field components in the straight section of this waveguide may be derived from two field components

$$E_y = \frac{1}{\epsilon_i(y)}\left(\beta^2 - \frac{\partial^2}{\partial x^2}\right)\phi^e \tag{1}$$

$$H_y = \left(\beta^2 - \frac{\partial^2}{\partial x^2}\right)\phi^h \tag{2}$$

where ϵ_i is the relative dielectric constant in each constituent region in Fig. 1, β is the propagation constant, and ϕ^e and ϕ^h are two scalar potentials. Since the structure is very similar to the image guide, we classify guided modes into E^y and E^x types. In the former E_y and H_x are predominant field components and we neglect H_y by setting $\phi^h = 0$. Next, we assume that the metal wall height h is reasonably large and the electromagnetic wave is reasonably well guided. Then, it is possible to neglect the fields in Regions 7 and 8 in Fig. 1. This assumption allows us to mathematically increase h to infinity. When this is done, we can divide the cross section into three vertical regions: 3 and 5, 1 and 2, and 4 and 6. We will apply the method of effective dielectric constants (EDC) to this hypothetical structure [3], [4]. The EDC, ϵ_{eD} of the central region (1 and 2) for the vertically polarized (E^y) modes, may be obtained from

$$\epsilon_{eD} = \epsilon_r - \left(\frac{k_y}{k_0}\right)^2 \tag{3}$$

where k_y is the solution to the eigenvalue equation

$$\frac{k_y}{\epsilon_r}\tan k_y b - \sqrt{(\epsilon_r - 1)k_0^2 - k_y^2} = 0. \tag{4}$$

Equation (4) is obtained by matching $H_x \sim \phi^e$ and $E_z \sim 1/\epsilon_i(y)\,\partial\phi^e/\partial y$ at the interface $y = b$ for a hypothetical slab structure realized by letting a approach infinity. The EDC's for 3 and 5, and 4 and 6 regions are assumed to be one.

Next, we replace the hypothetical structure with another hypothetical one, consisting of a vertical slab of width $2a$ and dielectric constant ϵ_{eD} sandwiched between air regions of width c which are in turn terminated by vertical metal walls at $x = \pm(a+c)$. Notice that we now have a vertical two dimensional structure which is closed in the sideward direction. By solving the eigenvalue equation of this final hypothetical structure for the phase constant k_x in the slab region, we obtain the propagation constant of the guided mode from

$$k_z = \sqrt{\epsilon_{ed}k_0^2 - k_x^2}\,. \tag{5}$$

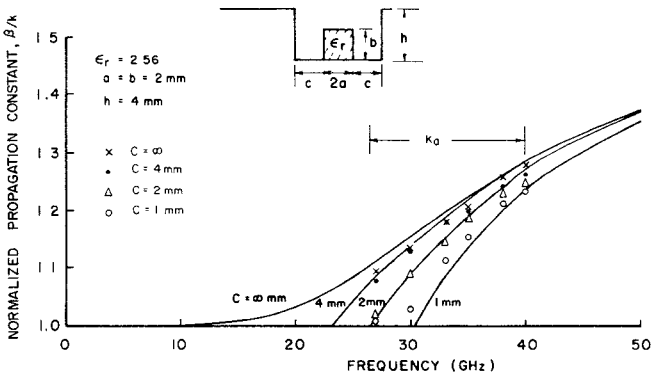

Fig. 3. Theoretical and experimental dispersion characteristics.

The method presented above is only an approximation. It is expected that the results are accurate at higher frequencies where the field is well guided. However, at lower frequencies, the results are less accurate because then the field extends to the Regions 7 and 8, and the assumption that h is infinite no longer applies.

Some numerical results are plotted in Fig. 3 on which experimental data are also indicated. In the computation, the value of c was varied and dispersion characteristics calculated. Also, the results for the ordinary image guide ($c \to \infty$) are included. It is noticed that all the results for the trapped image guide approach those for the image guide at higher frequencies because most of the energy is in the dielectric rod and the effect of the side walls becomes smaller. At lower frequencies the effect of the walls becomes significant. The propagation constant β approaches the cutoff value (free space wavelength k_0) faster than the image guide case. The smaller the value of c, the more pronounced the effect of the walls is. Actually, it is expected that the true value of β should be larger than the computed one near the cutoff, because there our assumption that h is infinite no longer holds. Such is clearly indicated by comparison between computed and experimental results for $c = 1$-mm case in the 25~30-GHz range. We also notice that all other experimental data qualitatively agree well with theoretical prediction. The experimental results at higher frequencies and those for image guides have some quantitative discrepancy with computed data. It is believed that the cause is in the experimental process which is quite sensitive to the perturbations applied to create standing wave patterns used to measure the guide wavelength.

Experimental results for transmission loss of a straight section of the waveguide are plotted in Fig. 4. The results include the loss and reflection at two transitions, each on both ends of the trapped image guide; one from the conventional metal waveguide to the image guide and another from the image guide to the trapped image guide. From Figs. 3 and 4, we find that the propagation characteristics are almost unaffected by the trough over 27~40 GHz if $c = 4$ mm. For smaller c values, the transmission loss increases at lower frequencies. This is because of larger scattering at transitions due to larger differences in

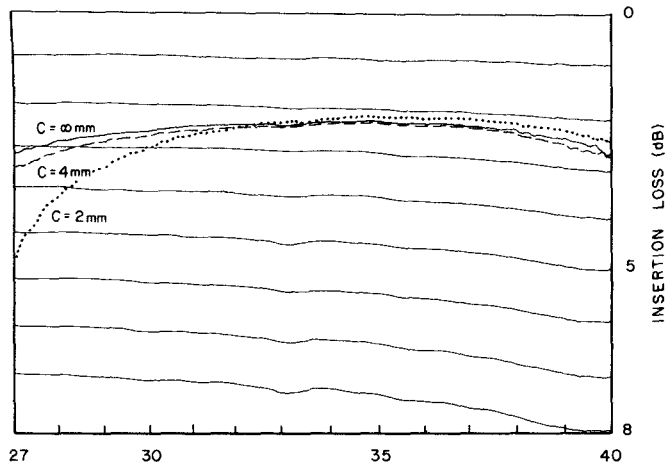

Fig. 4. Transmission loss in trapped image guides: the length between the transitions is 20cm.

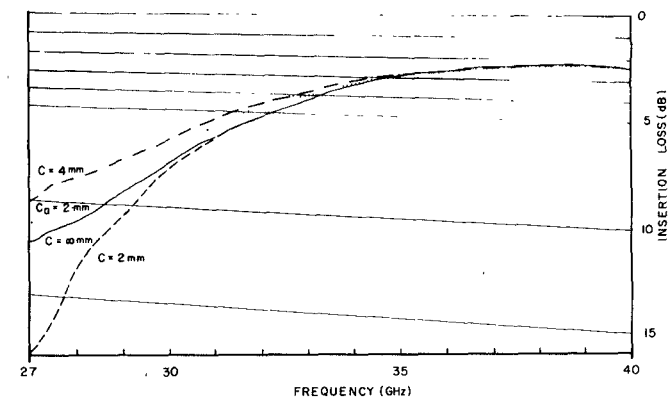

Fig. 5. Transmission loss in a curved section of the trapped image guide.

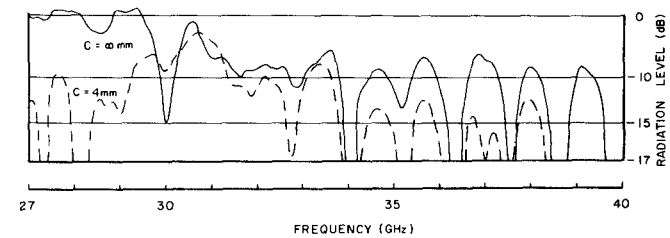

Fig. 6. Radiation loss from a curved section of the trapped image guide.

β between the image and trapped image guides. The scattering loss is largely in the form of radiation at the transition. However, no radiation has been detected from the trapped image guide section for any value of c.

III. Radiation at Curved Sections

Next, we investigated characteristics of a curved section of the trapped image guide. As an example, we used a 90° bend of center radius 63.7mm (Fig. 2(b)). The launchers from the metal to image guides are identical to the ones used for the measurement of the straight section. Similarly tapered transitions are used from the image guide to the trapped image guide. We studied the following setups: an image guide ($c\rightarrow\infty$) and trapped image guides of $c=2$ and 4mm. In the two latter cases, we also removed the inside walls of the trap, as we believe the radiation at the bend is generally directed to the outer side, or away from the center of the curvature. These two structures are labeled with a subscript a, such as c_a.

The transmission characteristics of a curved section are plotted in Fig. 5. It is noticed from the figure that, at lower frequencies where the effect of the trough is more pronounced, the transmission characteristics of the image guide are improved except for the $c=2$-mm case where it is believed that the scattering at the transition is quite strong. When we remove the inside wall, the loss decreases considerably as shown by $c_a=2$-mm curve. Since $c_a=4$-mm case is indistinguishable on the graph, only $c=4$-mm case is shown. Notice that the transmission characteristics in Fig. 5 include the scattering loss at transitions from the image guide to the trapped image guide.

Since radiation also occurs at the transition from the image guide to the trapped image guide, we find that the radiation loss caused in the curved section itself should be smaller than those in Fig. 5. To confirm our argument, we have measured two other quantities. The first is the reflection toward the microwave source from the dielectric waveguide setup including the transitions. The results indicate that the reflection is generally quite small (less than -20dB) and its characteristics do not depend on the different arrangement of the dielectric waveguide. This fact dictates that most of the energy scattered in the dielectric waveguide section is radiated and is not coupled to the metal waveguide mode through the transition.

The second quantity we measured is the radiated energy. Since the radiation occurs at several different locations, viz., at the transition to the image guide, at the image guide to trapped image guide transition and finally at the bend, it is desirable to distinguish these components. Although complete distinction is not possible, we tried to receive the energy radiated at the bend most strongly. To this end, we placed a standard gain horn at about 5cm away from the outer wall of the image guide wall location. The axis of the horn is on the radius of curvature intersecting the midpoint of the curved section. Therefore, the horn is looking at the setup in a symmetric manner.

Fig. 6 shows the frequency characteristics of the radiated power captured by the horn. Only the results for $c=4$-mm case and the image guide case ($c\rightarrow\infty$) are plotted to avoid crowded drawings as in the other cases, i.e., $c=2$, $c_a=2$, and $c_a=4$mm gave results similar to those for $c=4$-mm case. At lower frequencies, we see considerable reduction in radiation by the presence of the trough walls. It is, however, not possible to quantitatively compare different trapped image guide setups with each other, because radiations from several different sources are intermixed and the relative contributions from these sources will not be identical in each case.

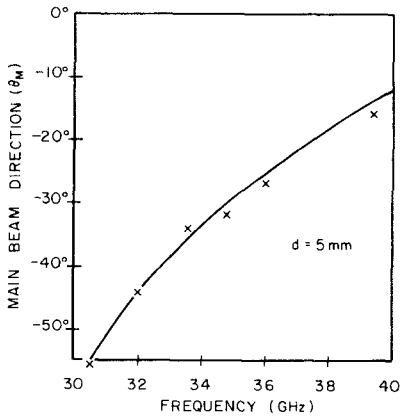

Fig. 7. Computed and measured (x) main beam direction.

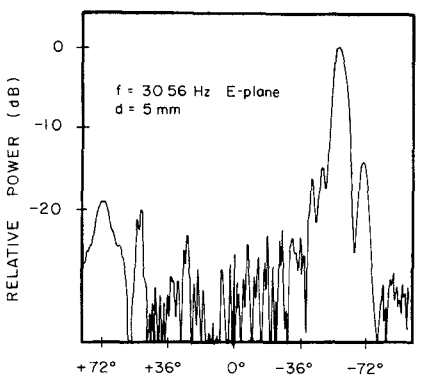

Fig. 8. Radiation pattern.

IV. Grating Leaky-Wave Structures

The new waveguide is still an open waveguide as the trough is not covered. It is well known that, when periodic perturbations (gratings) are created in an open waveguide, the resulting structure exhibits either the leaky wave or surface wave passband and stopband phenomena [5], [6].

The structure works as a frequency-scannable antenna if $|\beta_n/k_0|<1$ where k_0 is the free space wavenumber and $\beta_n=\beta+2n\pi/d$ is the propagation constant of the nth space harmonic associated with the grating with the period d. The main beam direction measured from the broadside is given by

$$\theta_M=\sin^{-1}\left(\frac{\beta}{k_0}+\frac{n\lambda}{d}\right). \tag{6}$$

Usually, n is taken to be -1. It is seen from (6) that θ_M is a function of frequency. If the attenuation of the guided wave due to radiation is small in the grating the radiation pattern is approximated by that of the cophasally excited linear array, and may be obtained from the well-known space factor calculation. Then, the power radiation is given by

$$S(\theta)=\frac{1}{N^2}\left|\frac{\sin(N\psi/2)}{\sin(\psi/2)}\right|^2 \tag{7}$$

$$\psi=k_0 d\sin\theta-\beta_n d \tag{8}$$

where N is the number of grating elements.

We developed an antenna from the trapped image guide with $\epsilon_r=2.56$, $a=b=2$mm, $h=4$mm, $c=4$mm. The grating period was taken as $d=5$mm and the number of elements was 28. The grating was created with narrow (1mm wide) metal strips placed on the top surface of the dielectric rod. Fig. 7 shows the computed and measured main beam directions when the frequency is changed in the *Ka* band. The negative values of θ_M imply that the antenna is backward firing. The differences in theory and experiments are mostly less than 2°. Fig. 8 shows a typical *E*-plane (yz-plane) radiation pattern. The pattern is a bit asymmetric as the antenna was placed near the edge of a big metallic slab. A relatively strong radiation in the +72° is caused by the fact that the transmitting oscillator radiated power directly into the feed horn of the antenna. The main beam width and sidelobe levels computed by the simple theory above resulted 6° (at −3dB) and −13.5dB as compared with measured values of 6.5° and −14dB.

V. Conclusions

We proposed a novel trapped image guide for millimeter wave applications for the purpose of reducing the radiation loss at curved sections. Fundamental propagation characteristics are obtained by an approximate theory. Numerical results are compared with measured data. Investigations of radiation loss at a 90° curved section as well as the application of this guide to a leaky-wave radiator are included.

References

[1] R. M. Knox, "Dielectric waveguide microwave integrated circuits—An overview," *IEEE Trans. Microwave Theory Tech.*, vol. MTT-24, pp. 806–814, Nov. 1976.

[2] H. Jacobs, G. Novick, C. M. LoCascio, and M. M. Chrepta, "Measurement of guide wavelength in rectangular dielectric waveguides," *IEEE Trans. Microwave Theory Tech.*, vol. MTT-24, pp. 815–820, Nov. 1976.

[3] W. McLevige, T. Itoh, and R. Mittra, "New waveguide structures for millimeter wave and optical integrated circuits," *IEEE Trans. Microwave Theory Tech.*, vol. MTT-23, pp. 788–794, Oct. 1975.

[4] T. Itoh, "Inverted strip dielectric waveguide for millimeter-wave integrated circuits," *IEEE Trans. Microwave Theory Tech.*, vol. MTT-24, pp. 821–827, Nov. 1976.

[5] T. Itoh, "Applications of gratings in a dielectric waveguide for leaky-wave antennas and band-reject filters," *IEEE Trans. Microwave Theory Tech.*, vol. MTT-25, pp. 1134–1137, Dec. 1977.

[6] B. S. Song and T. Itoh, "Distributed Bragg reflection dielectric waveguide oscillators," *IEEE Trans. Microwave Theory Tech.*, vol. MTT-27, pp. 1019–1022, Dec. 1979.